RSC Advances

This article can be cited before page numbers have been issued, to do this please use: C. Liang, H. Ren, C. Li, D. Yin and J. Liu, *RSC Adv.*, 2016, DOI: 10.1039/C6RA17756E.

ROYAL SOCIETY OF CHEMISTRY

www.rsc.org/advances

View Article Online
DOI: 10.1039/C6RA17756E

Journal Name

ARTICLE

Pd@MIL-101 as an efficient bifunctional catalyst for hydrodeoxygenation of anisole

Received 00th January 20xx,
Accepted 00th January 20xx

DOI: 10.1039/x0xx00000x

www.rsc.org/

Hangxing Ren, Chuang Li, Dongdong Yin, Jinxuan Liu and Changhai Liang*

A series of highly porous acidic metal-organic framework MIL-101 supported Pd nanoparticles materials with different Pd contents were prepared through a simple sol-gel method. The obtained heterogeneous catalytic material Pd@MIL-101 was comprehensively characterized by powder X-ray diffraction (PXRD), N_2 adsorption, FTIR spectroscopy of pyridine adsorption (Py-IR) and transmission electron microscope (TEM). The intact crystallinity of MIL-101 was found before and after Pd loading process, and Pd nanoparticles with diameter of 2 - 3.5 nm were found homogeneously dispersed in MIL-101. The bifunctional Pd@MIL-101 catalyst exhibits good activity in hydrodeoxygenation (HDO) of anisole. It has been shown that the reaction temperature and the Pd content play important roles in the activity toward oxygen-removal. The catalyst after reaction at high temperature of 240 °C revealed that the Pd nanoparticles tended to migrate to the external surface of the MOF materials and form larger aggregates.

1. Introduction

Metal-organic frameworks (MOFs) have attracted tremendous attention because of their high surface area and porosity, nanoscale cavities as well as tunable chemical functionality.[1] The diverse properties of MOFs make them potential candidates to be used in various applications such as gas storage, separation, heterogeneous catalysis and photoelectric conversion.[2-5] Heterogeneous catalysis is one of the most important applications for MOFs with active catalytic sites arising from the metal or organic molecules (or both).[6] The capacity to insert functional groups into porous MOFs with well-defined channels is imperative for heterogeneous catalysis.[7] Formation of recyclable heterocatalyst by encapsulation of metal nanoparticles (NPs) into MOF cavities are of current interests, because the crystalline porous MOFs architectures can efficiently limit the migration and aggregation of metal NPs, which makes MOFs as appropriate support/host matrix for metal NPs.[8, 9] A large number of MOF-supported noble metal NPs have been investigated as active heterogeneous catalysts.[10-14] Taking into account the diversity and rich functionalities of MOFs, the design of metal@MOF bifunctional (metal-acid/base) or multifunctional cooperative catalyst carries huge potentials in utilizing the encapsulated metal active sites together with the coordinatively unsaturated sites of MOF as Lewis acid active sites or MOF bearing Brønsted acid and base functionalities via in-situ one-step synthesis or diverse post-synthesis functionalization or guest encapsulation.[15]

MIL-101, a chromium-based MOF with the empirical formula $Cr_3(F,OH)(H_2O)_2O[(O_2C)C_6H_4(CO_2)]_3$, possesses large specific surface area (BET, ca. 4000 $m^2\ g^{-1}$), huge porosity (ca. 2.0 $cm^3\ g^{-1}$) and high thermal (up to 275 °C) as well as chemical stability to water and common organic solvents.[16] These outstanding features make MIL-101 an excellent support for hosting small metal NPs. In addition, MIL-101 possesses numerous coordinatively unsaturated chromium sites (CUSs), which can provide Lewis acid sites upon removal of the terminal water molecules.[17-19] These Lewis acidic sites has been demonstrated to play significant roles in promoting the reactivity of aromatic hydrocarbons due to the easy adsorption of aromatic rings by Lewis acids, and the acidic MIL-101 can be used to construct bifunctional or multifunctional metal organic framework catalysts by encapsulating another species.[20-22] Pd NPs immobilized in MIL-101 has also been shown to be a high-efficient bifunctional Lewis acid@hydrogenation catalyst for one-step synthesis of methyl isobutyl ketone, one-pot synthesis of menthol from citronellal reactions and selective aqueous hydrogenation of phenols.[23-25] However, researches on hydrodeoxygenation performance of oxy-compound using a bifunctional Pd@MIL-101 catalyst are rather scarce.

Hydrodeoxygenation (HDO) of anisole, a methoxy-rich lignin model compound, has been extensively investigated in biofuel production from bio-oil upgrading.[26] Various heterocatalysts have been developed for HDO of bio-oil.[27-29] In previous studies, Al_2O_3 supported CoMo- and NiMo-based sulfide catalysts have been reported to show higher activity than other catalysts for HDO of bio-oil, whereas the Al_2O_3 support was unstable in the presence of large amounts of water，and

Laboratory of Advanced Materials and Catalytic Engineering, Institute of Artificial photosynthesis, State Key Laboratory of Fine Chemicals, Dalian University of Technology, Dalian 116024, China. E-mail: changhai@dlut.edu.cn;
Fax: +86 411 84986353; Tel: +86 411 84986353
Electronic Supplementary Information (ESI) available: [details of any supplementary information available should be included here]. See DOI: 10.1039/x0xx00000x

View Article Online
DOI: 10.1039/C6RA17756E

usually resulted in coke formation.[30-32] Recently, noble metals (e.g., Pt, Rh, and Pd), base metals (e.g., Ni and Cu), metal phosphides and carbides have been used in HDO of model compounds of bio-oils.[33-37] Among the well-established metal-based catalysts, noble metals exhibit better performance compared to Mo-based sulfide catalysts with respect to the hydrocarbon yield and deoxygenation level.[38] Moreover, noble metal catalysts do not require the use of environmentally unfriendly sulfur, which make them particular interest for the development of environment friendly catalysts. It is worth noting that bifunctional catalysts comprising of a metal function and an acid function have been shown to improve HDO activity dramatically compared to the metal catalyst alone.[33, 39] A dual-functional catalyst using Pd/C with a liquid acid (H_3PO_4) catalyst has been reported for the HDO of phenolic bio-oils and it stated that the presence of dual catalytic functions which are metal-catalyzed hydrogenation and acid-catalyzed dehydration both needed for the overall HDO.[39] However, it is difficult for the recovery of the acid from the reaction mixture. Using of acidic support instead of extra liquid acid is better for the recovery and reuse of the catalyst and important for the development of heterogeneous catalysis. The acidity of the support has been proved to play a key role in improving the catalytic behavior and product distributions by facilitating the hydrogenolysis of oxy-compound and transmethylation.[40-42] Therefore, designing of new bifunctional catalysts capable of maintaining stability during the on-stream conditions of bio-oil hydrotreatment becomes of interest.

Rational control of metal NPs can enhance the catalyst performance and well-defined nano-scale metal catalysts have exhibited numerous applications in the field of biomass conversion.[43] Pd NPs are well-known as the effective catalysts for numerous selective hydrogenation and oxidation reactions and many supported Pd NPs have been reported.[44-46] In this study, we loaded Pd into porous MIL-101 with controlled size and investigated the hydrodeoxygenation of the lignin monomer anisole with the dual-functional noble Pd NPs and acidic MIL-101 catalyst. The high surface area and pore volume of MIL-101 has been demonstrated to enhance metal dispersion, leading to an improved hydrogenation capability and the acid sites of the MIL-101 support were expected to accelerate the hydrogenolysis of anisole.

2. Experimental

2.1 Catalyst preparation

Preparation of MIL-101: MIL-101(Cr) was synthesized from hydrothermal reaction according to the reported procedures by Férey et al. with a simple post-processing.[16] In a typical synthesis, 0.64 g of terephthalic acid was slowly added to 19.2 g of de-ionized water under stirring, then 1.6 g of $Cr(NO_3)_3{\cdot}9H_2O$ and 0.16 g of hydrofluoric acid were added subsequently and kept stirring for 15 min. The mixture was then transferred to a Teflon-lined autoclave and heated at 220 °C for 8 h in a convection oven. After the reaction, the mixture was cooled naturally to room temperature. The resulting green solid product was filtered using a large pore fritted glass filter (G2) firstly to remove the white needle crystals of residual terephthalic acid and then isolated from the solution by centrifugal separation. The resulting solid was washed by de-ionized water to eliminate other unreacted ions. Then the as-synthesized MIL-101 was purified sequentially through N,N-Dimethylformamide (2 times) and ethanol (2 times) treatments and the centrifugal separation, after which the product was dried under vacuum at 150 °C for 12 h.

Preparation of Pd@MIL-101: MIL-101 supported palladium nanoparticles were synthesized via a sol-gel method.[47] In brief, polyvinyl alcohol (PVA) used as a protecting agent was dissolved by hot water and then added to an aqueous solution of $PdCl_2$ (1×10^{-3} mol L^{-1}) (PVA monomer/metal = 10 : 1 molar ratio) under vigorous stirring and kept stirring for 1 h in the condition of ice bath. Then, a freshly prepared aqueous of $NaBH_4$ ($NaBH_4$/metal = 5 : 1 molar ratio, 0.1 mol L^{-1}) was added to obtain a dark brown PVA-Pd nano-sol, after which the water dispersed MIL-101 was added immediately to the colloids and stirred at 0 °C for another 4 h. Finally, the sample was washed by deionized water for several times and dried under vacuum at 100 °C for 2 h, followed by heating at 200 °C in H_2 for 2 h to remove excess of PVA.

2.2 Catalyst Characterization

Powder X-ray diffraction (PXRD) patterns of the samples were obtained by a D/MAX-2400 diffractometer using Cu Kα radiation (40 kV, 100 mA, λ=1.5418 Å). The surface area, pore volume, and pore size distribution of MIL-101 and Pd@MIL-101 materials were determined from nitrogen adsorption-desorption isotherms at -196 °C using a Quantachrome Autosorb-IQ apparatus. Before the nitrogen adsorption, the sample was degassed at 200 °C for 10 h. The content of Pd was measured by inductively coupled plasma-atomic emission spectroscopy (ICP-AES) (Perkin-Elmer Optima 2000 DV). The particle size and distribution of the samples were analyzed by transmission electron microscopy (TEM) (JEM-2000EX, 120 kV). Powder samples were ultrasonicated in ethanol and dispersed on TEM copper grids. The acid sites of the materials were characterized by using FTIR spectroscopy of pyridine adsorption (Py-IR), recorded on an EQUIOX-55 Fourier transform infrared spectrometer (Bruker, German) at a resolution of 4 cm^{-1}. The sample placed in the IR cell was evacuated at 200 °C for 1 h and then cooled to 50 °C to record the background spectra before the adsorption of pyridine. Then the sample with saturated pyridine was evacuated at 100 °C for 50 min before scanning the sample spectra and 200 °C for 20 min similarly.

2.3 Anisole HDO and product analysis

Anisole HDO was carried out in a 50 mL batch reactor. Before the reaction, the catalysts were reduced by Ar : H_2 = 2 : 1 at 200 °C for 2 h, and then passivated under Ar overnight. The freshly prepared catalysts (0.06 g) and 20 mL reactants of anisole (8 wt%, 1.2 g) dissolved in n-decane with an internal

View Article Online
DOI: 10.1039/C6RA17756E

standard of n-dodecane (2 wt%) for quantitative GC analysis were rapidly introduced into the batch reactor. The reactor was flushed with H_2 for 3 times, after which the catalytic hydrodeoxygenation was conducted at 240 °C and 3 MPa of hydrogen pressure. Upon reaction completion, the catalyst particles were removed from the solution by centrifuge. The products were analyzed by gas chromatograph (GC-7890F, FID, FFAP column 30 m × 0.32 mm × 0.5 μm).

3. Results and discussion

3.1 Characterization of MOF materials

The powder XRD patterns of the synthesized MIL-101 materials are shown in Fig. 1. The characteristic diffraction peaks of MIL-101 were detected before and after the metal Pd NPs loading, indicating that the structure of MIL-101 was retained regardless of the loaded metal content in the materials. However, no obvious characteristic signal for Pd NPs was detected, which is owing to the low content of Pd or small particle sizes.[23]

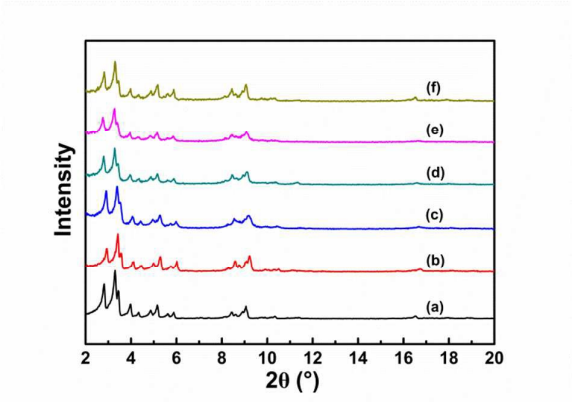

Fig. 1 Powder XRD patterns of MIL-101 samples: (a) MIL-101; (b)-(e) 0.5, 2.0, 3.3, 4.1 wt% Pd@MIL-101; (f) 4.1 wt% Pd@MIL-101 after reaction.

The N_2 adsorption isotherms of MIL-101 and Pd@MIL-101 are shown in Fig. 2 and the specific surface area and porosity are summarized in Table 1. Type I isotherms according to IUPAC classification are observed, a typical feature for materials with microporous structures. The as-synthesized MIL-101 exhibited a Brunauer-Emmett-Teller (BET) surface area of 2839 m^2 g^{-1} and a pore volume of 1.44 cm^3 g^{-1}. A gradual decrease of surface area and pore volume with loaded Pd NPs suggested that the mesoporous MIL-101 are occupied by highly dispersed Pd NPs, an obvious decrease of micropore area should come from the collapse of partial framework and some Pd NPs passing through the porous windows and occupying partial pores.[14] The pore size distribution curves (calculated by DFT method) showed an obvious decrease of the pore diameter centered on 1 - 3.5 nm after Pd loading, which can be attributed to the introduction of Pd particles into the pore and the residual protecting agent PVA after 200 °C heating treatment on the gas adsorption capacities of the catalysts.[47]

The size and dispersion of Pd NPs were characterized by TEM (Fig. 3). It can be seen that small spherical Pd particles were homogeneously distributed in MIL-101. The particle size distribution showed that the majority of the Pd particles have the size of 2 - 3.5 nm for the 0.5 wt% Pd@MIL-101 sample corresponding to the two mesoporous cavities (2.9 nm and 3.4 nm) of MIL-101. However, very few amounts of Pd NPs still remained outer surface because of the electrostatic interactions between MIL-101(Cr) and palladium.[48] A certain amount of bigger particles (larger than 4 nm) were observed when the Pd loading amount reached to 4.1 wt%. These particles beyond the size of MOF cavities were assumed to locate on the outside surface of MIL-101. But there might be another case, particles larger than the crystallographic cavity dimensions formed inside the cavities when two or more cavities were occupied by a single nanoparticle or if partial destruction of the framework occurred in the process of loading nanoparticles.[8]

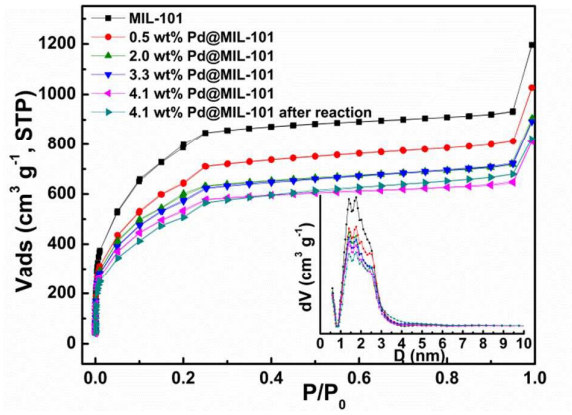

Fig. 2 N_2 adsorption-desorption isotherms with DFT pore distributions (derived from the adsorption branches of the isotherms) of MIL-101 and Pd@MIL-101 before and after reaction.

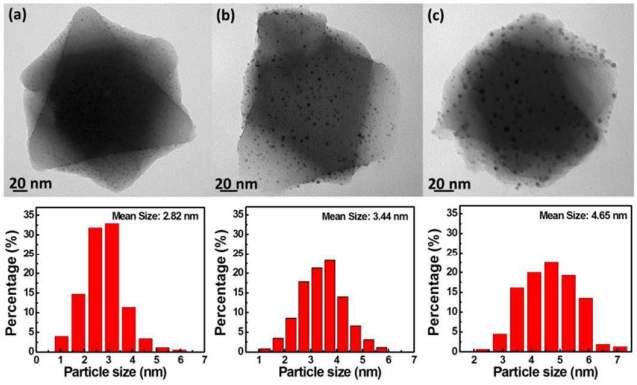

Fig. 3 TEM images of 0.5 wt% Pd@MIL-101 (a), 4.1 wt% Pd@MIL-101 before (b) and after (c) reaction and their corresponding size distribution of Pd nanoparticles.

FTIR experiments were carried out to check the surface acidity of activated MIL-101 by using pyridine as probe

View Article Online
DOI: 10.1039/C6RA17756E

molecules. As shown in Fig. 4, an intense band at 1451 cm^{-1} was observed after pyridine absorption, suggesting the existence of Lewis acidic sites on activated MIL-101 after the removal of terminal water molecules. After Pd NPs were introduced into MIL-101, the pyridine stretching at 1451 cm^{-1} decreased dramatically, which indicated that Pd NPs or the protecting agent PVA were coordinated to the chromium (III) CUSs, hindering the absorption of pyridine on Cr^{3+} sites. The same results were also obtained by Qin et al. with a little shifting of Lewis acid center characteristic peak to 1445 cm^{-1}.[49]

3.2 Catalytic activity

As a model reaction, the HDO of methoxy-rich compound anisole has been selected for the investigation over the prepared Pd@MIL-101catalysts with different Pd contents at 240 °C under 3 MPa pressure. Fig. 5 shows the variation of the conversion of anisole and the yield of products in terms of reaction time. The main products detected by GC were cyclohexyl methyl ether (CME), cyclohexanol (CHL) and cyclohexane (CHN). In addition, small amounts of phenol (PHE) and cyclohexanone (CHOE) originating from direct demethylation of anisole and subsequent hydrogenation were also detected. The stronger C-O bond strength of the RO-Ar with a value about 422 kJ mol^{-1} than that of the RO-R (339 kJ mol^{-1}) implies that the cleavage of RO-Ar is more difficult than that of RO-R.[50] Therefore, removal of oxygen from anisole will be enhanced by hydrogenation of the aromatic ring to the corresponding cycloalkane.

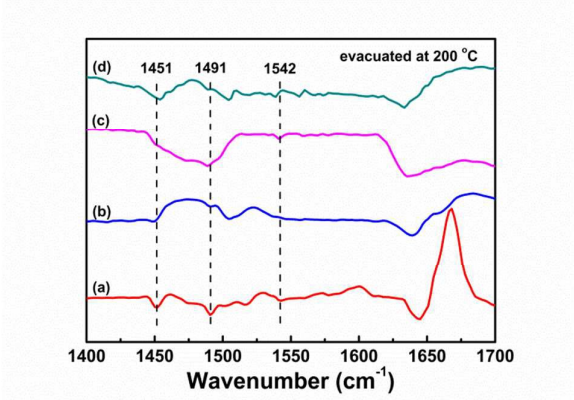

Fig. 4 Py-IR spectra of MIL-101 and Pd@MIL-101 samples evacuated at 200 °C after introduction of an equilibrium pressure of pyridine, MIL-101 (a), 3.3 wt% Pd@MIL-101 (b), 4.1 wt% Pd@MIL-101 before (c) and (d) after reaction.

In Fig. 5 the main products obtained from anisole are displayed, including aromatic ring-hydrogenated CME along with subsequently demethylated CHL in the first 2 hours, which indicates that the palladium-catalyzed aromatic ring-hydrogenation is involved during the first step in HDO of anisole. A relatively high deoxygenation rate was achieved to yield more CHN with longer time, revealing that deoxygenation is more difficult during the hydrotreating of anisole. Herein, a hydrogenation-deoxygenation mechanism is preferred in the HDO of anisole.[38, 51] Three steps are proposed during the HDO process (Scheme 1). First, the aromatic ring of anisole was hydrogenated to corresponding saturated cyclohexyl methyl ether. Second, the methoxy group was demethylated to generate cyclohexanol by the hydrogenolysis of the O-CH_3 bond. Finally, cyclohexanol was deoxygenated to yield cyclohexane by the intramolecular dehydration reaction of hydroxyl group. The Lewis acid chromium (III) sites in MIL-101 may have an interaction with oxygenated functional group of anisole or cyclohexyl methyl ether thus accelerate the cleavage of O-CH_3, which can be proved by the fact that phenol was generated when using pure MIL-101 as a catalyst in HDO of anisole (Table 2).

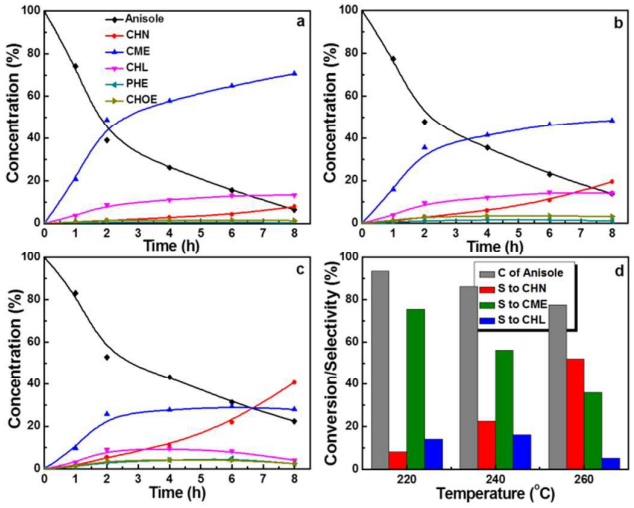

Fig. 5 Variation of the conversion of anisole and the yield of products with time over 3.3 wt% Pd@MIL-101, (a) 220 °C, (b) 240 °C, (c) 260 °C, and (d) temperature dependence of conversion and selectivity to main products, 3 MPa, 8 h.

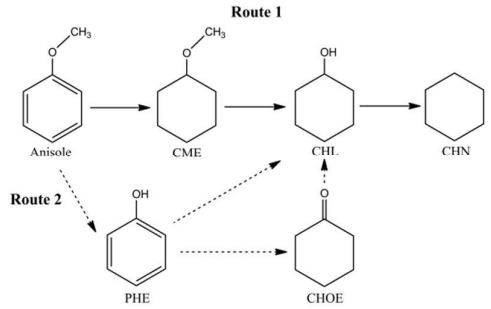

Scheme 1. Reaction network of anisole hydrodeoxygenation over Pd@MIL-101 catalysts.

We have investigated the effect of temperature on the product distribution and effectiveness of the overall process (Fig. 5). The increase of the reaction temperature from 220 °C to 260 °C leaded to a remarkable change in the product distribution, presenting a significant increase of CHN selectivity accompanied by a decrease of CME selectivity. The result above suggests that hydrogenation of unsaturated aromatic

View Article Online
DOI: 10.1039/C6RA17756E

ring smoothly proceed at low temperature, whereas further hydrodeoxygenation would require a higher temperature. However, the conversion of anisole decreased along with the rise of temperature, which probably because the aggregated Pd NPs due to the removal and decomposition of protecting agent PVA at higher temperature, since the aggregation of Pd NPs was confirmed by the TEM results of 4.1wt% Pd@MIL-101 catalyst (Fig. 3). As a result, the number of activity sites for hydrogenation is decreased resulting in the reduction of the generation rate of CME, and the increase of the yield of deoxygenated CHN, suggests that the catalyst has no degradation in activity in this case.

The pressure dependence of conversion and selectivity toward main products over 4.1 wt% Pd@MIL-101 is shown in Fig. 6. With the hydrogen pressure increasing from 1.0 to 3.0 MPa, the conversion of anisole increased from 19% to 76%. Under high hydrogen pressure, it favors the route of hydrogenation saturation of aromatic ring and the following deoxygenation process. Nevertheless, more PHE was generated at low hydrogen pressure, explaining the ease of ArO-R bond cleavage.

Table 1 N_2 physisorption results of the MIL-101 and Pd@MIL-101 samples

Sample	S_{BET} ($m^2\ g^{-1}$)	MA[a] ($m^2\ g^{-1}$)	EA[b] ($m^2\ g^{-1}$)	MV[c] ($cm^3\ g^{-1}$)	TV[d] ($cm^3\ g^{-1}$)
MIL-101	2839	2616	223	1.22	1.44
0.5 wt% Pd@MIL-101	2353	2085	268	0.99	1.26
2.0 wt% Pd@MIL-101	2110	1898	212	0.89	1.11
3.3 wt% Pd@MIL-101	2064	1782	282	0.84	1.11
4.1 wt% Pd@MIL-101	1916	1738	178	0.82	1.10
4.1 wt% Pd@MIL-101 after reaction	1864	1544	320	0.74	1.05

[a] Micropore area. [b] External surface area. [c] Micropore volume. [d] Total volume.

Table 2 Results of the HDO of anisolea over MIL-101 and Pd@MIL-101 catalyst

Catalyst	T (°C)	P (MPa)	Conversion (%)	Selectivity (%)				
				CHN	CME	CHL	PHE	CHOE
MIL-101	240	3	7.2	--	--	--	>99	--
0.5 wt% Pd@MIL-101	240	3	23.7	11.2	29.2	19.7	34.5	5.4
2.0 wt% Pd@MIL-101	240	3	87.8	17.4	65.4	12.7	1.2	3.4
3.3 wt% Pd@MIL-101	220	3	93.5	8.3	75.5	14.3	0.4	1.5
3.3 wt% Pd@MIL-101	240	3	86.3	22.5	56.2	16.3	1.3	3.7
3.3 wt% Pd@MIL-101	260	3	77.7	52.1	35.9	5.3	3.3	3.4
4.1 wt% Pd@MIL-101	240	1	19.0	2.9	15.6	7.8	45.1	28.6
4.1 wt% Pd@MIL-101	240	2	52.2	32.0	29.1	14.6	14.6	10.6
4.1 wt% Pd@MIL-101	240	3	76.2	30.8	52.4	9.8	4.1	2.7

[a] Reaction conditions: 1.2 g anisole, 0.06 g catalyst, 600 rpm stirring speed, 8 h, 50 mL batch reactor.

The highly dispersed Pd particles exhibited excellent hydrogenation activity since a large amount of CME was obtained, and the reaction activity was enhanced with the increase of palladium content (Table 2). However, a longer reaction time or a higher temperature was needed to accelerate the deoxygenation process of the cyclic compounds. It should be noted that the high selectivity to CME than CHN indicates a higher adsorption selectivity toward the aromatic rings compared to the oxygen atom of the saturated cyclic compounds. It seemed that the best catalyst was 3.3 wt% Pd@MIL-101 under the existing conditions in consideration of the conversation and the yield of oxygen-free CHN. However, the conversion of anisole decreased when the palladium content increased to 4.1 wt%, which is attributed to the aggregation of palladium NPs with a large amount of palladium loading (Fig. 3).

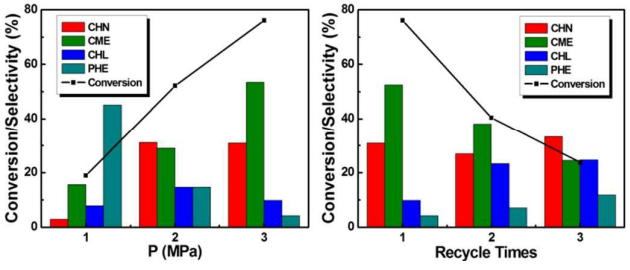

Fig. 6 Pressure dependence of conversion and selectivity toward main products in HDO of anisole (left) and the recyclability of 4.1 wt% Pd@MIL-101 catalyst (right), 240 °C, 8 h.

View Article Online
DOI: 10.1039/C6RA17756E

The recovery and reuse of the catalyst are important issues to evaluate a catalyst. The recyclability test results are shown in Fig. 6. All the experiments were performed under the same reaction conditions as described above. The catalyst was washed with ethanol, and then heated at 80 °C under vacuum, followed by reduction at 200 °C for 2 h under the atmosphere of Ar : H_2 = 2 : 1. It can be seen in Fig. 6, the conversion of anisole was obviously decreased after the first circle, and the selectivity of CME had a significantly decrease but no decrease of the CHN selectivity was observed.

To further study the recyclability of the Pd@MIL-101 catalyst, the used Pd@MIL-101 catalyst was further characterized with XRD, N_2 adsorption, TEM and Py-IR. As shown in Fig. 1, there was no apparent loss of crystallinity in XRD patterns after the reaction process, indicating that the structure of MIL-101 remained intact and the catalyst is tolerable to water generated form the dehydration of cyclohexanol to cyclohexane. The N_2 adsorption amount of the used Pd@MIL-101 has virtually no change compared with the freshly prepared catalyst, but a significant reduce in the micropore area together with the substantially increased external surface area were observed in Table 1, which is due to partly damage of MIL-101 crystal structure. The TEM analysis revealed that the size of Pd NPs increased, and the resulted large Pd NPs were mainly located on the external surface of MIL-101 of the used catalyst. A slight damage of the octahedral structure of MIL-101 can well explain the N_2 adsorption results with reduced internal and increased external surface areas (Fig. 3). Based on Dhakshinamoorthy's work[8], the metal NPs are located within the MOF cavity rather than diffuse outer surface due to size limitation to cross the windows in tri-directional MOFs; whereas MOFs with a pore system with channels are less appropriate candidates to act as hosts because the NPs can freely move through the channel and eventually can meet other NPs and grow further or migrate to the external surface. In any case, some Pd particles migrated to the surface during catalysis and formed larger aggregates in the tri-directional MIL-101 at relatively high temperature, which results in a reduction of hydrogenation capacity toward unsaturated aromatic ring. The intensity of characteristic band at 1451 cm^{-1} for Lewis acid center in the used catalyst increased compared to the fresh catalyst, which is attributed to the aggregation of Pd NPs and the re-exposing of unsaturated chromium (III) sites (Fig. 4).

4. Conclusions

The embedding of palladium nanoparticles into the acidic metal-organic framework MIL-101 has been successfully prepared by a sol-gel method. The combination of the MIL-101 (as Lewis acid catalytic sites) and Pd NPs (as hydrogenation catalyst sites) afford an interesting bifunctional catalyst with a very high BET surface area and huge pore volume. The TEM images showed that Pd particles were well dispersed in MIL-101 with size of 2 - 3.5 nm. The Pd@MIL-101 catalyst can efficiently catalyze the HDO of anisole with excellent hydrogenation activity toward aromatic compounds and promoted hydrogenolysis of C-O by the interaction of Lewis acid and oxygen atom. The catalyst is tolerable to water and can maintain its structure after few circles. But the high temperature can result in the aggregation of Pd particles, thus lead to an activation declination. The present findings offer the new opportunities in the development of bifunctional Pd@MIL-101 catalyst, further optimization of the catalyst preparation to obtain highly stabilized Pd particles to against aggregation is underway.

Acknowledgements

We gratefully acknowledge the financial support provided by the National Natural Science Foundation of China (21573031 and 21428301) and the Fundamental Research Funds for the Central Universities (DUT15ZD106 and DUT15RC(4)09).

Notes and references

1. G. Ferey, *Chem. Soc. Rev.*, 2008, **37**, 191-214.
2. W. Qin, W. Cao, H. Liu, Z. Li and Y. Li, *RSC Adv.*, 2014, **4**, 2414-2420.
3. J.-R. Li, R. J. Kuppler and H.-C. Zhou, *Chem. Soc. Rev.*, 2009, **38**, 1477-1504.
4. A. Dhakshinamoorthy, M. Opanasenko, J. Cejka and H. Garcia, *Catal. Sci. Technol.*, 2013, **3**, 2509-2540.
5. J. Liu, W. Zhou, J. Liu, I. Howard, G. Kilibarda, S. Schlabach, D. Coupry, M. Addicoat, S. Yoneda, Y. Tsutsui, T. Sakurai, S. Seki, Z. Wang, P. Lindemann, E. Redel, T. Heine and C. Wöll, *Angew. Chem. Int. Ed.*, 2015, **54**, 7441-7445.
6. J. Lee, O. K. Farha, J. Roberts, K. A. Scheidt, S. T. Nguyen and J. T. Hupp, *Chem. Soc. Rev.*, 2009, **38**, 1450-1459.
7. P. Silva, S. M. F. Vilela, J. P. C. Tome and F. A. Almeida Paz, *Chem. Soc. Rev.*, 2015, **44**, 6774-6803.
8. A. Dhakshinamoorthy and H. Garcia, *Chem. Soc. Rev.*, 2012, **41**, 5262-5284.
9. H. R. Moon, D.-W. Lim and M. P. Suh, *Chem. Soc. Rev.*, 2013, **42**, 1807-1824.
10. F. Schröder, D. Esken, M. Cokoja, M. W. E. van den Berg, O. I. Lebedev, G. Van Tendeloo, B. Walaszek, G. Buntkowsky, H.-H. Limbach, B. Chaudret and R. A. Fischer, *J. Am. Chem. Soc.*, 2008, **130**, 6119-6130.
11. A. Aijaz, T. Akita, N. Tsumori and Q. Xu, *J. Am. Chem. Soc.*, 2013, **135**, 16356-16359.
12. L. Chen, H. Chen and Y. Li, *Chem. Commun.*, 2014, **50**, 14752-14755.
13. A. Aijaz and Q. Xu, *J. Phys. Chem. Lett.*, 2014, **5**, 1400-1411.
14. M. Zhang, Y. Yang, C. Li, Q. Liu, C. T. Williams and C. Liang, *Catal. Sci. Technol.*, 2014, **4**, 329-332.
15. S. Bhattacharjee, C. Chen and W.-S. Ahn, *RSC Adv.*, 2014, **4**, 52500-52525.
16. G. Férey, C. Mellot-Draznieks, C. Serre, F. Millange, J. Dutour, S. Surblé and I. Margiolaki, *Science*, 2005, **309**, 2040-2042.
17. Y. K. Hwang, D.-Y. Hong, J.-S. Chang, S. H. Jhung, Y.-K. Seo, J. Kim, A. Vimont, M. Daturi, C. Serre and G. Férey, *Angew. Chem. Int. Ed.*, 2008, **47**, 4144-4148.
18. Y. K. Hwang, D.-Y. Hong, J.-S. Chang, H. Seo, M. Yoon, J. Kim, S. H. Jhung, C. Serre and G. Férey, *Appl. Catal. A.*, 2009, **358**, 249-253.

View Article Online
DOI: 10.1039/C6RA17756E

19. A. Henschel, K. Gedrich, R. Kraehnert and S. Kaskel, *Chem. Commun.*, 2008, 4192-4194.
20. H. Liu, Y. Li, H. Jiang, C. Vargas and R. Luque, *Chem. Commun.*, 2012, **48**, 8431-8433.
21. J. Juan-Alcañiz, E. V. Ramos-Fernandez, U. Lafont, J. Gascon and F. Kapteijn, *J. Catal.*, 2010, **269**, 229-241.
22. F. G. Cirujano, A. Leyva-Pérez, A. Corma and F. X. Llabrés i Xamena, *ChemCatChem*, 2013, **5**, 538-549.
23. Y. Pan, B. Yuan, Y. Li and D. He, *Chem. Commun.*, 2010, **46**, 2280-2282.
24. F. G. Cirujano, F. X. Llabres i Xamena and A. Corma, *Dalton Trans.*, 2012, **41**, 4249-4254.
25. H. Liu, Y. Li, R. Luque and H. Jiang, *Advanced Synthesis & Catalysis*, 2011, **353**, 3107-3113.
26. H. Wang, J. Male and Y. Wang, *ACS Catal.*, 2013, **3**, 1047-1070.
27. K. L. Deutsch and B. H. Shanks, *Appl. Catal. A.*, 2012, **447–448**, 144-150.
28. M. V. Bykova, D. Y. Ermakov, V. V. Kaichev, O. A. Bulavchenko, A. A. Saraev, M. Y. Lebedev and V. A. Yakovlev, *Appl. Catal. B*, 2012, **113–114**, 296-307.
29. L. Wang, C. Li, S. Jin, W. Li and C. Liang, *Catal. Lett.*, 2014, **144**, 809-816.
30. A. Centeno, E. Laurent and B. Delmon, *J. Catal.*, 1995, **154**, 288-298.
31. D. C. Elliott, *Energ. Fuels*, 2007, **21**, 1792-1815.
32. C. V. Loricera, B. Pawelec, A. Infantes-Molina, M. C. Álvarez-Galván, R. Huirache-Acuña, R. Nava and J. L. G. Fierro, *Catal. Today*, 2011, **172**, 103-110.
33. X. Zhu, L. L. Lobban, R. G. Mallinson and D. E. Resasco, *J. Catal.*, 2011, **281**, 21-29.
34. H. Ohta, H. Kobayashi, K. Hara and A. Fukuoka, *Chem. Commun.*, 2011, **47**, 12209-12211.
35. C. R. Lee, J. S. Yoon, Y.-W. Suh, J.-W. Choi, J.-M. Ha, D. J. Suh and Y.-K. Park, *Catal. Commun.*, 2012, **17**, 54-58.
36. S. Jin, Z. Xiao, C. Li, X. Chen, L. Wang, J. Xing, W. Li and C. Liang, *Catal. Today*, 2014, **234**, 125-132.
37. K. Li, R. Wang and J. Chen, *Energ. Fuels*, 2011, **25**, 854-863.
38. J. Wildschut, F. H. Mahfud, R. H. Venderbosch and H. J. Heeres, *Industrial & Engineering Chemistry Research*, 2009, **48**, 10324-10334.
39. C. Zhao, J. He, A. A. Lemonidou, X. Li and J. A. Lercher, *J. Catal.*, 2011, **280**, 8-16.
40. V. N. Bui, D. Laurenti, P. Delichère and C. Geantet, *Appl. Catal. B*, 2011, **101**, 246-255.
41. T. Prasomsri, A. T. To, S. Crossley, W. E. Alvarez and D. E. Resasco, *Appl. Catal. B*, 2011, **106**, 204-211.
42. A. Popov, E. Kondratieva, J. M. Goupil, L. Mariey, P. Bazin, J.-P. Gilson, A. Travert and F. Maugé, *J. Phys. Chem. C*, 2010, **114**, 15661-15670.
43. Y. Wang, S. De and N. Yan, *Chem. Commun.*, 2016, **52**, 6210-6224.
44. Q. Wang, X. Cai, Y. Liu, J. Xie, Y. Zhou and J. Wang, *Appl. Catal. B*, 2016, **189**, 242-251.
45. W. Niu, Y. Gao, W. Zhang, N. Yan and X. Lu, *Angew. Chem. Int. Ed.*, 2015, **54**, 8271-8274.
46. B. Zhang, Y. Yuan, K. Philippot and N. Yan, *Catal. Sci. Technol.*, 2015, **5**, 1683-1692.
47. G. Chen, S. Wu, H. Liu, H. Jiang and Y. Li, *Green Chemistry*, 2013, **15**, 230-235.
48. Y. Huang, Z. Lin and R. Cao, *Chem. Euro. J.*, 2011, **17**, 12706-12712.
49. L. Qin, Z. Li, Z. Xu, X. Guo and G. Zhang, *Appl. Catal. B*, 2015, **179**, 500-508.
50. E. Furimsky, *Appl. Catal. A.*, 2000, **199**, 147-190.
51. J. Wildschut, I. Melián-Cabrera and H. J. Heeres, *Appl. Catal. B*, 2010, **99**, 298-306.

View Article Online
DOI: 10.1039/C6RA17756E

Journal Name

ARTICLE

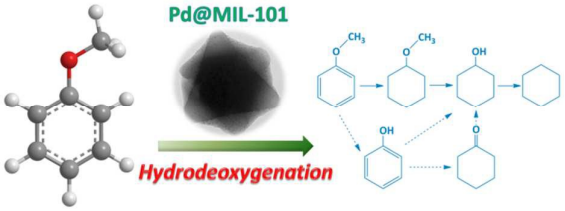

Pd@MIL-101 with highly dispersed Pd particles exhibits high activity for hydrodeoxygenation of anisole as bifunctional catalytic materials.